Inorganic Chemistry

pubs.acs.org/IC

Article

Observation of Enhanced Long-Range Ferromagnetic Order in B-Site Ordered Double Perovskite Oxide Cd_2CrSbO_6

Shengjie Liu,◆ Xiao Wang,◆ Zunyi Deng, Xubin Ye, Zhao Pan, Dabiao Lu, Haoting Zhao, Jie Zhang, Maocai Pi, Zhiwei Hu, Chien-Te Chen, Cheng Dong, Yao Shen, Tian Cui, Yanping Huang, Jiawang Hong,* Zhenhua Chi,* and Youwen Long*

Cite This: *Inorg. Chem.* 2024, 63, 19964−19971

Read Online

ACCESS | Metrics & More | Article Recommendations

ABSTRACT: A B-site ordered double perovskite oxide Cd_2CrSbO_6 was synthesized under high-pressure and high-temperature conditions. The compound crystallizes to a monoclinic structure with a space group of $P2_1/n$. The charge configuration is confirmed to be that of $Cd^{2+}/Cr^{3+}/Sb^{5+}$. The magnetic Cr^{3+} ions form a tetrahedral structural frustrated lattice, while a long-range ferromagnetic phase transition is found to occur at T_C = 16.5 K arising from the superexchange interaction via the Cr−O−Cd−O−Cr pathway. Electrical transport measurements indicate that Cd_2CrSbO_6 is an insulator that can be described by the Mott 3D variable range hopping mechanism. First-principles calculations reproduce well the ferromagnetic and insulating ground state of Cd_2CrSbO_6 with an energy band gap of 1.55 eV. The intrinsic ferromagnetic insulating nature qualifies Cd_2CrSbO_6 as a promising candidate for possible spintronics applications.

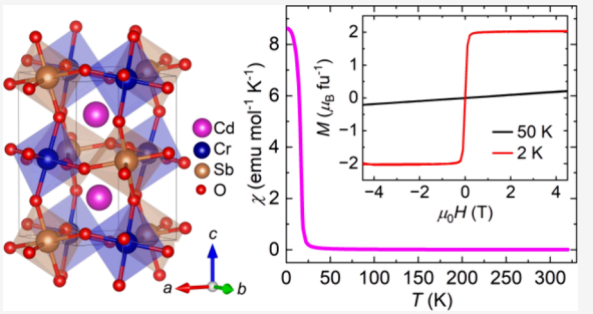

1. INTRODUCTION

B-site ordered double perovskite oxide with the chemical formula $A_2BB'O_6$ derivates from the simple ABO_3 perovskite oxide with two different cations occupying at the B-site in a rock salt fashion.[1] The flexibility of the site occupancy enables it to exhibit a wide variety of physical properties, such as giant magnetoresistance,[2] multiferroicity,[3] exchange bias,[4] and high-T_C ferromagnetism.[5] Recently, the B-site ordered double perovskite oxide with only one magnetic cation residing at the B-site has attracted much attention, owing to the subtle magnetic ground state. In such a structure, the sole magnetic B-site cation is located in an edge-shared tetrahedral lattice, as shown in Figure 1a. This geometric magnetic frustration usually prevents the formation of long-range magnetic order.[6−19]

Exceptionally, A_2CrSbO_6 (A = Sr and Ca) provides rare examples that exhibit long-range spin order in an edge-shared tetrahedral lattice with space group $P2_1/n$, as depicted in Figure 1a,b. Specifically, Sr_2CrSbO_6 experiences a long-range antiferromagnetic (AFM) transition at T_N = 12 K.[20] However, Ca_2CrSbO_6 shows a long-range ferromagnetic (FM) order at T_C = 13 K.[21] Theoretical calculations indicated that the tilting of the Cr/SbO_6 octahedra is critical for the formation of long-range spin order, and a change in sign of the nearest-neighbor Cr−Cr magnetic coupling was identified with Cr−O−Sb angle decreasing from 169.2 to 152.5°, which is responsible for the AFM to FM transition from Sr_2CrSbO_6 to Ca_2CrSbO_6.[22]

Interestingly, a recent study indicates that for double perovskite oxides, the frustration factor ($f = |\theta|/T_N$, where θ is the Weiss temperature and T_N is the Néel temperature) is linearly dependent on the tolerance factor.[23] Thus, the stabilization of the long-range spin ordering with an enhanced critical temperature is expected to occur in the A_2CrSbO_6 system if a smaller-size cation occupies the A-site.

In this paper, we report a novel B-site ordered double perovskite oxide Cd_2CrSbO_6 (CCSO) synthesized using high-pressure and high-temperature techniques, which enable a smaller cation of Cd occupying at the A-site, thus obtaining a crystal structure with more heavily tilted BO_6 octahedra.[4,24−26] Similar to Ca/Sr_2CrSbO_6, CCSO also crystallizes to a monoclinic $P2_1/n$ space group with valence states of $Cd^{2+}/Cr^{3+}/Sb^{5+}$. However, an enhanced T_C of 16.5 K was found to occur in CCSO, resulting from heavier Cr/SbO_6 octahedral tilting with a smaller Cr−O−Sb bond angle of 147.5°. An insulating state was also identified by electrical transport measurements. First-principles calculations further confirmed the insulating ferromagnetic state of CCSO with a spin

Received: August 20, 2024
Revised: September 25, 2024
Accepted: October 1, 2024
Published: October 10, 2024

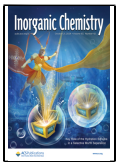

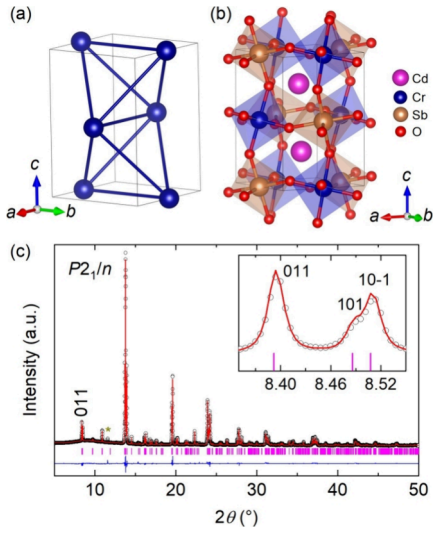

Figure 1. (a) Edge-shared tetrahedral lattice of Cr in CCSO. (b) Crystal structure of CCSO composed of alternating CrO_6 and SbO_6 octahedra by sharing corner O atoms. (c) SXRD pattern and Rietveld refinement of CCSO. Black circles, red lines, and blue lines indicate the observed, calculated, and difference, respectively. Magenta ticks indicate the allowed Bragg reflections for space group $P2_1/n$. Inset displays the pattern near the (011) peak. Asterisk indicates minor unknown impurities.

moment of 3.0 μ_B/Cr^{3+} and an energy gap of 1.55 eV, making CCSO promising for possible spintronics applications.[27−30]

2. EXPERIMENTAL DETAILS

High purity (>99.9%) CdO, Cr_2O_3, and Sb_2O_5 with a mole ratio of 4:1:1 were thoroughly ground with an agate mortar and then encapsulated into a platinum capsule of 3 mm diameter and 4 mm length. These procedures were carried out in a glovebox full of argon due to the toxicity of CdO and the chemical instability of CdO and Sb_2O_5 in air. The capsule was then processed with a cubic-anvil-type high-pressure apparatus. The sample was slowly pressurized to 9 GPa and then heated at 1375 K for 30 min. After the high-pressure sintering process, the temperature was quenched to room temperature and then the pressure was slowly released to ambient pressure within 10 h.

Powder synchrotron X-ray diffraction (SXRD) was collected at the BL02B2 (λ = 0.65 Å) beamline of SPring-8. The 2θ scan was from 5 to 50° with a step of 0.006°. The Rietveld refinement was performed using the GSAS software.[31] The X-ray absorption spectra (XAS) at the Cr-$L_{2,3}$ edges were obtained at room temperature at the TLS11A beamline of the National Synchrotron Radiation Research Center (NSRRC), via total electron yield mode. The magnetic susceptibility and isothermal magnetization were performed with a Quantum Design superconducting quantum interference device magnetometer (MPMS-VSM). For the magnetic susceptibility measurements, both zero-field-cooling (ZFC) and field-cooling (FC) modes were adopted under a magnetic field of 0.1 T. The resistivity and specific heat were measured using a Quantum Design physical property measurement system (PPMS-9T).

First-principles calculations were performed based on the density functional theory (DFT) within the Vienna ab initio simulation package (VASP),[32−34] with the projector augmented wave (PAW) potentials[35] to describe the electron−ionic core interaction. After testing different electron correlation methods and the onsite Coulomb interaction for the localized 3d orbitals, the Perdew−Burke−Ernzerhof formulation for solid (PBEsol)[36] of the generalized gradient approximation (GGA) was chosen to describe the exchange−correlation interaction of electrons. The effective Hubbard U = 5 eV was adopted for the Cr d orbital.[22] The wave functions are expanded in a plane wave basis set with an energy cutoff of 520 eV. The force on each ion is converged to be less than 0.001 eV/Å, and a precision of 10^{-6} eV is adopted to minimize the total energy of the system. A 7 × 7 × 5 k-mesh in the Monkhorst−Park scheme in reciprocal space was used to ensure convergence for the total energy self-consistent calculations. The Cd $4d^{10}5s^2$, Sb $5s^25p^3$, Cr $3d^54s^1$, and O $2s^22p^4$ electrons were treated as valence electrons. VESTA software was used for visualization of crystal structures.[37]

3. RESULTS AND DISCUSSION

Figure 1c shows the SXRD pattern and the Rietveld refinements of CCSO. The SXRD data can be well refined using the monoclinic $P2_1/n$ (No. 14) space group with a = 5.3496(3) Å, b = 5.4498(3) Å, c = 7.6668(4) Å, and β = 90.157(1)°, as displayed in Figure 1b. The (011) Bragg peak (inset of Figure 1c) clearly indicates the rock salt order of Cr and Sb at the B and B′ sites, respectively. The refined parameters are listed in Table 1. No visible antisite occupation for Cr/Sb was found to occur. Via the bond valence sum (BVS) calculations,[38] the valence states of 2.01, 2.99, and 4.74 were obtained for Cd, Cr, and Sb, respectively, suggesting the charge combination to be $Cd^{2+}{}_2Cr^{3+}Sb^{5+}O_6$, in agreement with charge conservation and the XAS measurements shown below.

It is well-known that XAS at the $L_{2,3}$ edges are very sensitive to the valence states and local environments for 3d transition metals. For an opened d shell, an increase of the valence by one will lead to a 1−2 eV shift of the white line of the X-ray absorption spectrum toward higher photon energies, accompanied by a significant variation of the spectral line shape.[5,26,39]

Table 1. Rietveld Refinement Results of CCSO[a]

atom	site	x	y	z	U_{iso} (100 × Å^2)
Cd	4e	0.9917(2)	0.0408(1)	0.2511(1)	0.73(1)
Cr	2d	0.5	0	0	0.12(4)
Sb	2c	0	0.5	0	0.45(1)
O1	4e	0.0966(7)	0.4618(7)	0.2459(7)	0.15(10)
O2	4e	0.6968(9)	0.2953(9)	0.0486(8)	0.57(16)
O3	4e	0.1985(9)	0.1910(9)	0.9467(8)	0.25(15)
Cd−O (Å)	2.363(4); 2.244(4); 2.610(5); 2.274(5); 2.681(6); 2.712(6); 2.219(5); 2.619(5); **BVS:** 2.01				
Cr−O (Å)	2.028(5)(×2); 1.958(5)(×2); 1.962(5)(×2); **BVS:** 2.99				
Sb−O (Å)	1.964(5)(×2); 2.004(5)(×2); 2.033(5)(×2); **BVS:** 4.74				
∠Cr−O−Sb (°)	147.6(2); 148.8(3); 145.8(3)				

[a]Space group is $P2_1/n$ (No. 14) with lattice parameters of a = 5.3496(3) Å, b = 5.4498(3) Å, c = 7.6668(4) Å, and β = 90.157(1)°. R_{wp} = 4.35%, R_p = 3.21%. BVS values (V_i) were calculated using the formula $V_i = \Sigma_j S_{ij}$, and $S_{ij} = exp[(r_0 - r_{ij})/0.37]$ with r_0 = 1.904 Å for Cd, r_0 = 1.724 Å for Cr and r_0 = 1.912 Å for Sb.

https://doi.org/10.1021/acs.inorgchem.4c03543
Inorg. Chem. 2024, 63, 19964−19971

To further ascertain the valence state for Cr, XAS measurements at the Cr-$L_{2,3}$ edges were performed. As shown in Figure 2, one finds that the white line shape and peak position of the Cr-$L_{2,3}$ of CCSO resemble those of the reference $Cr^{3+}{}_2O_3$, confirming the presence of the Cr^{3+} state in CCSO.

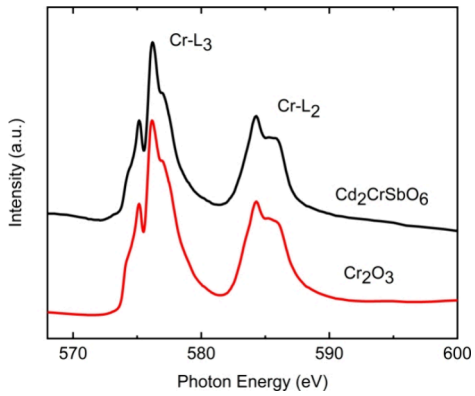

Figure 2. XAS at the Cr-$L_{2,3}$ edges of CCSO. Cr_2O_3 was used as a Cr^{3+} reference.

Now, we turn to investigate the magnetic properties of CCSO. Figure 3a depicts the temperature-dependent magnetic susceptibility measured at 0.1 T with both ZFC and FC modes between 2 and 320 K. One finds that the ZFC and FC curves almost overlap, and both curves experience a sharp elevation at a critical temperature T_C = 16.5 K, which can be clearly identified by a sharp peak of the first-order derivative ZFC curve, as shown in the inset of Figure 3a. Since there is only one type of magnetic ion Cr^{3+} occupying one Wyckoff position in CCSO, a ferromagnetic state below T_C is assigned. As shown in Figure 3a, the reciprocal magnetic susceptibility (χ) can be well fitted with the Curie–Weiss law at temperatures above 40 K using the formula $(\chi - \chi_0)^{-1} = (T - \theta)/C$, yielding the Weiss temperature θ = 16.3 K. The positive θ indicates the dominated FM interactions in CCSO, and the value of θ is in agreement with the experimental T_C = 16.5 K. On the basis of the fitted Curie constant C = 1.478 emu mol^{-1}, the effective magnetic moment is calculated to be μ_{eff} = 3.44 μ_B $f.u.^{-1}$ ($= \sqrt{8C}$). This value is comparable with the spin-only theoretical value of 3.87 μ_B $f.u.^{-1}$ (S = 3/2 for Cr^{3+}). Figure 3b displays the field-dependent magnetization measured at different temperatures. The linear $M(H)$ curve above T_C is indicative of the paramagnetic state. Below T_C, e.g., at 2 K, a saturated magnetic moment of 2.05 μ_B $f.u.^{-1}$ is observed, which is smaller than the theoretical value (3 μ_B/Cr^{3+}). This discrepancy may be attributed to the noncolinear FM alignment of Cr^{3+} spins and/or the presence of some antiphase boundaries as often observed in double perovskite oxides.[1]

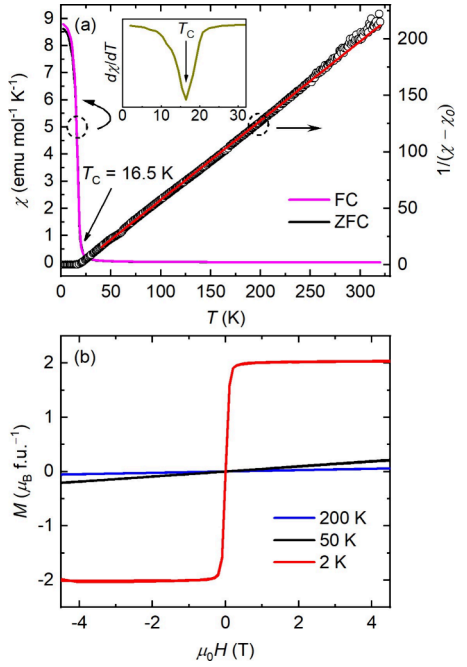

Figure 3. (a) Temperature-dependent magnetic susceptibility of CCSO. Both ZFC (black line) and FC (magenta line) modes are shown. Reciprocal magnetic susceptibility (black circles) and the Curie–Weiss fitting (red line) above 40 K with the formula $(\chi - \chi_0)^{-1} = (T - \theta)/C$ are shown. Inset shows the first-order derivative of the ZFC curve. (b) Field-dependent magnetization of CCSO at selected temperatures.

We further investigated the specific heat of CCSO. As shown in Figure 4a, with decreasing temperature to T_C, the specific heat shows a sharp λ-type anomaly. Additionally, when external magnetic fields are applied, the anomaly shifts to higher temperatures and changes to a broad hump, in accordance with the long-range FM transition. On the other hand, as depicted in Figure 4b, the experimental data of specific heat can be well fitted by using the function $C_P = \alpha T^{3/2} + \beta T^3$ below 7 K, with fitting parameters α = 75.6 mJ mol^{-1} $K^{-5/2}$ and β = 3.12 mJ mol^{-1} K^{-4}. Here, the $T^{3/2}$ and T^3 terms, respectively, indicate the ferromagnetic excitation and phonon contributions, whereas the absence of the temperature linear term suggests the lack of conducting electrons. The specific heat data thus suggest the FM insulating nature of the CCSO.

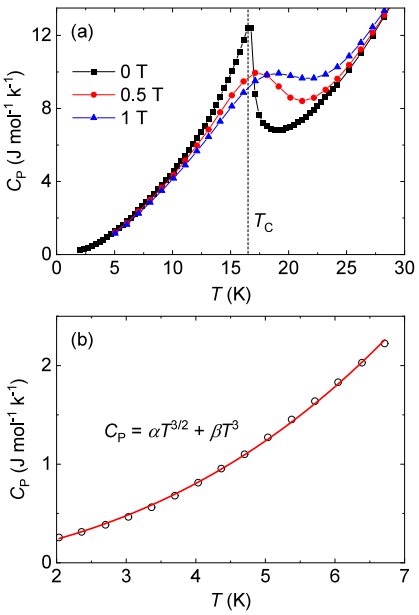

Figure 4. (a) Temperature-dependent specific heat of CCSO under selected magnetic fields. Vertical dashed line indicates T_C. (b) Experimental heat capacity below 7 K (black circles) and fitting with formula $C_P = \alpha T^{3/2} + \beta T^3$ (red line).

https://doi.org/10.1021/acs.inorgchem.4c03543
Inorg. Chem. 2024, 63, 19964−19971

To evaluate the magnetic entropy, as shown in Figure 5a, the lattice contribution to the specific heat was obtained by

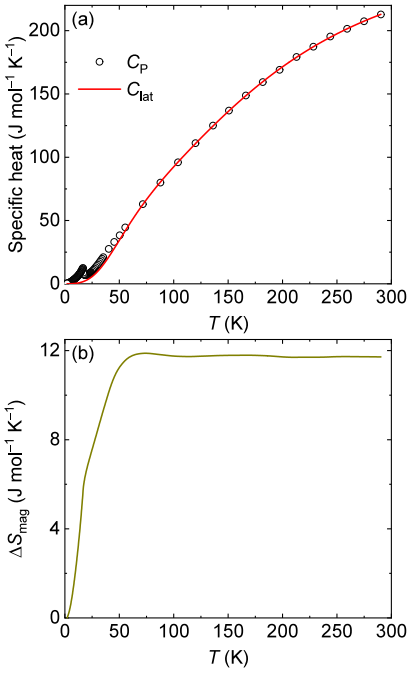

Figure 5. (a) Temperature-dependent specific heat of CCSO measured at zero magnetic field (black circles) and the Einstein-Debye fitting above 70 K (red line). (b) Temperature-dependent magnetic specific heat and magnetic entropy of CCSO.

performing the fitting of the C_P above 70 K using the Einstein−Debye equation[40,41]

$$C_{lat} = a \times \frac{9R}{(T_D/T)^3}\int_0^{T_D/T}\frac{x^4 e^x}{(e^x-1)^2}dx + b \times 3R\frac{(T_E/T)^2 e^{T_E/T}}{(e^{T_E/T}-1)^2},$$

where R = 8.314 J mol^{-1} K^{-1} is the universal gas constant, a and b are the number of vibrating modes per formula unit, and T_D and T_E are the Debye and Einstein temperatures, respectively. The fitting yields a = 5.3, b = 5.7, T_D = 304 K, and T_E = 725 K. As shown in Figure 5b, the magnetic entropy $\Delta S_{mag} = \int \frac{C_P - C_{lat}}{T} dT$ was calculated to be 11.69 J mol^{-1} K^{-1}, in good agreement with the theoretical value R ln(2S + 1) = 11.53 J mol^{-1} K^{-1}, where S = 3/2 is the spin quantum number of Cr^{3+}.

Figure 6 displays the temperature-dependent electrical resistivity (ρ) of CCSO. The ρ gradually increases with decreasing temperature, indicating an insulating or semiconducting feature. Furthermore, the ln $\rho - T^{-1/4}$ curve was plotted, as shown in the inset of Figure 6. Two linear regions can be observed in 70−350 K and below T_C, respectively. The resistivity data in both temperature regions can be well fitted using a Mott three-dimensional variable range hopping (VRH) mechanism[42] with the equation $\rho = \rho_0 \times \exp(T_0/T)^{1/4}$, where T_0 represents the characteristic temperature and ρ_0 is a constant. The fitted T_0 is 545 and 3960 K for the higher and lower temperature region, respectively. The larger T_0 value below T_C may be ascribed to the magnetic scattering and the decreases in the density of states near the Fermi surface of the insulative FM state.

To get deeper insights into the electronic structures and magnetic properties of CCSO, first-principles theoretical calculations were carried out based on DFT. The experimental

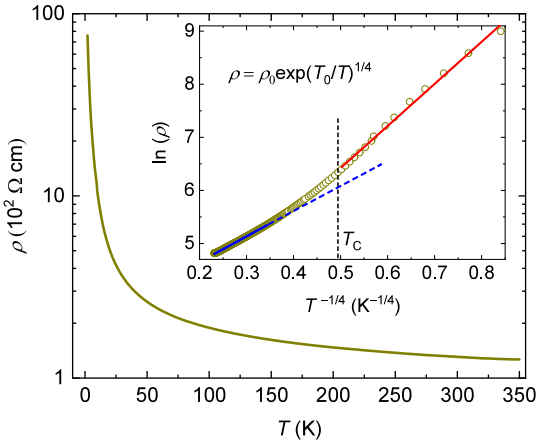

Figure 6. Temperature-dependent resistivity of CCSO. Inset displays the experimental data (circles) and the fitting with a Mott three-dimensional VRH model at temperatures below T_C (red line), and 70−350 K (blue line) and its extension to T_C (dashed blue line). Vertical dashed line indicates T_C.

lattice parameters from the SXRD refinement data were used as the initial structure, and after full relaxation, the optimized lattice parameters are a = 5.383 Å, b = 5.492 Å, c = 7.720 Å, and β = 90.22° for numerical calculations. After various atomic magnetic configurations were tried, the system with the lowest energy is the ferromagnetic state with magnetic moments in the same direction, which is consistent with our experimental results. As shown in Figure 7a, there is no density of electronic state near the Fermi level, and the band gaps are 1.55 and 2.00 eV for spin-up and spin-down electrons, respectively. As depicted in Figure 7b, the conduction band is mainly contributed by Cr d electrons, and the valence band is a hybrid of O p electrons and Cr d electrons. The magnetic moment for each Cr atom is 3.030 μ_B based on theoretical calculations.

To obtain further insight into the magnetic coupling in CCSO, the strengths of the nearest neighboring exchange interactions J_1 and J_3, and the next nearest neighboring exchange interaction J_2 were examined. As depicted in Figure 8a,b, the Cr−Cr distances for J_1, J_2, and J_3 interaction are 5.400, 7.664, and 5.410 Å, respectively. The Heisenberg model was employed to express the total energy within a 2 × 2 × 1 supercell, as a sum of a nonmagnetic part with energy E_0 and magnetic parts given by the equation, $H = E_0 - \sum_{i<j} J_{ij} S_i \cdot S_j$. Four magnetic configurations were constructed to find out the system energy and FM interactions of J_1 = 0.583 meV and J_3 = 0.959 meV and a much weaker AFM interaction of J_2 = −0.003 meV were obtained.

Figure 8c displays the 3D magnetic charge density of Cr in CCSO, which presents a typical $t_{2g}^3 e_g^0$ electronic structure, where the magnetic charge isosurface around the Cr atom has a cube-like shape, with eight angles protruding outward and six faces recessed inward. Meanwhile, an induced magnetic moment in the 2p state appears around the adjacent O atom. Therefore, in the process of forming the compound, each Cr atom loses three electrons to form the +3 valence state. Further, the octahedral crystal field splits the 3d states of a free Cr atom approximately into low lying t_{2g} triplet and high lying e_g doublet for spin-up channels. According to Hund's rules, the remaining three electrons around Cr occupy the t_{2g}

https://doi.org/10.1021/acs.inorgchem.4c03543
Inorg. Chem. 2024, 63, 19964−19971

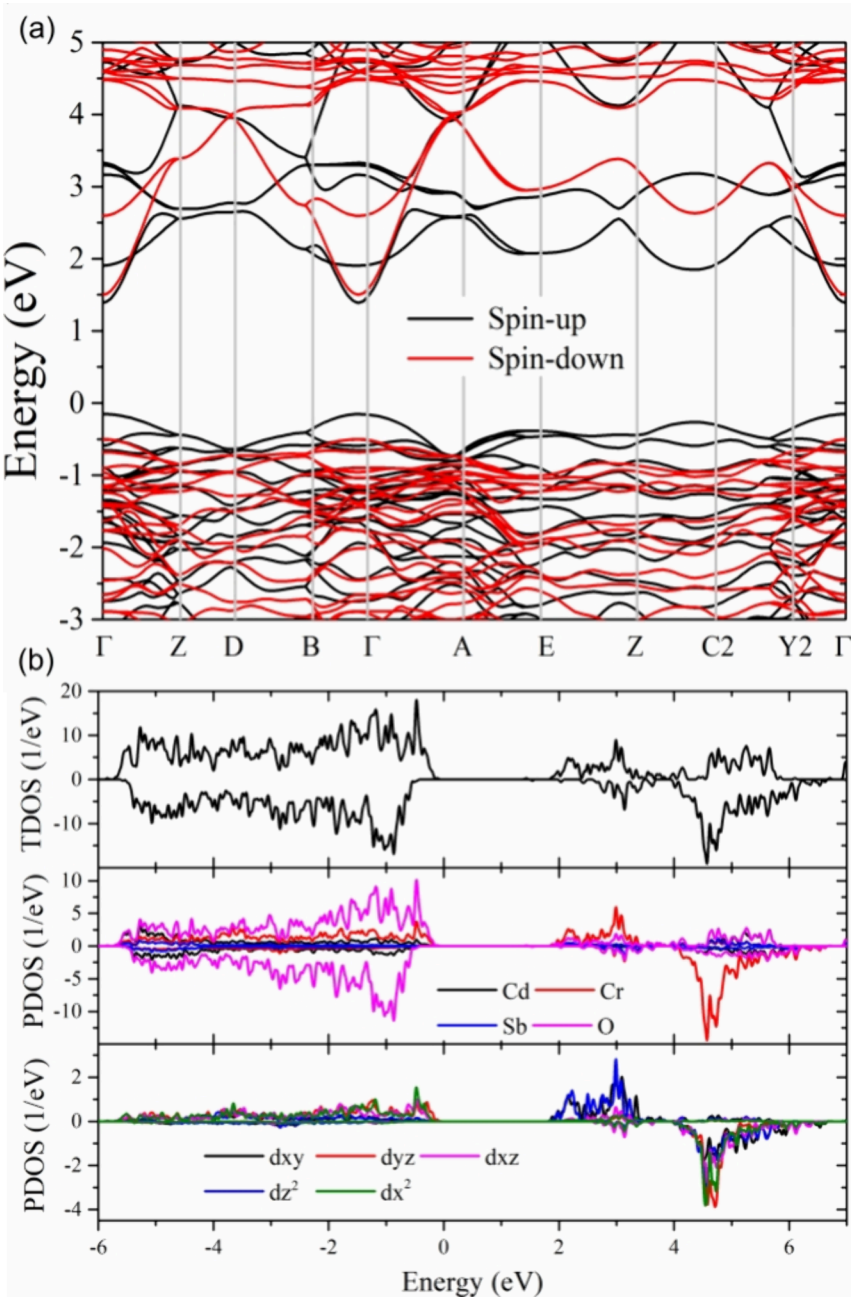

Figure 7. (a) Electronic band structure and (b) density of states of CCSO. Positive and negative values in (b) represent spin-up and spin-down electronic state densities, respectively.

orbital and exhibit the same spin arrangement, as depicted in Figure 8d.

Compared with Ca_2CrSbO_6, which has comparable absolute values between $J_1 \sim 0.1$ meV and $J_2 \sim -0.05$ meV,[22] a prominent enhancement of the J_1 (J_3) is obtained for CCSO, where the strength of the FM coupling is larger than that of the AFM one by 1 order of magnitude, leading to the enhancement of T_C from 13 K in Ca_2CrSbO_6 to 16.5 K in the current CCSO. It is worth noting that in similar tetrahedral magnetic structures, for example, Sr_2CaReO_6,[6] Sr_2MgReO_6,[7] Sr_2MnSbO_6,[18] and Sr_2FeTaO_6[19] show spin-glass behaviors at low temperatures; Ba_2LnSbO_6 and Sr_2LnSbO_6 (Ln = Dy, Ho, and Gd) do not form long-range magnetic ordering with temperature down to 2 K;[15] Sr_2CuTeO_6 has a spin-liquid-like ground state;[17] and Ba_2NaOsO_6,[8] Ba_2YMoO_6,[9] La_2LiMoO_6,[9] and $A_2BB'O_6$ (A = Ba, La, B = Y, Li, B′ = Ru, Re)[10−13] have T_N lower than their θ, as a result of the considerable magnetic frustration. However, the current CCSO provides a rare example of long-range FM order with θ being very close to T_C.

Now, we discuss how the Cr/SbO_6 tilting enhances the T_C and stabilizes the FM state in CCSO. According to previous theoretical calculations,[22] in Sr_2CrSbO_6 with slight CrO_6 tilting as characterized by the Cr−O−Sb bond angle of 169.2°, the O $2p_x$ and $2p_y$ orbitals bend toward the A-site Sr, leading to the formation of the long-range superexchange coupling pathway Cr−O−Sr−O−Cr. Considering the half-filled t_{2g} state of Cr^{3+}, virtual hopping $t_{2g}\uparrow$-$t_{2g}\downarrow$ results in an AFM state for Sr_2CrSbO_6. With CrO_6 octahedra further tilting so that the Cr−O−Sb bond angle decreases to 152.5° in Ca_2CrSbO_6, the significant distortion of the Cr/SbO_6 chains can give rise to a

https://doi.org/10.1021/acs.inorgchem.4c03543
Inorg. Chem. 2024, 63, 19964−19971

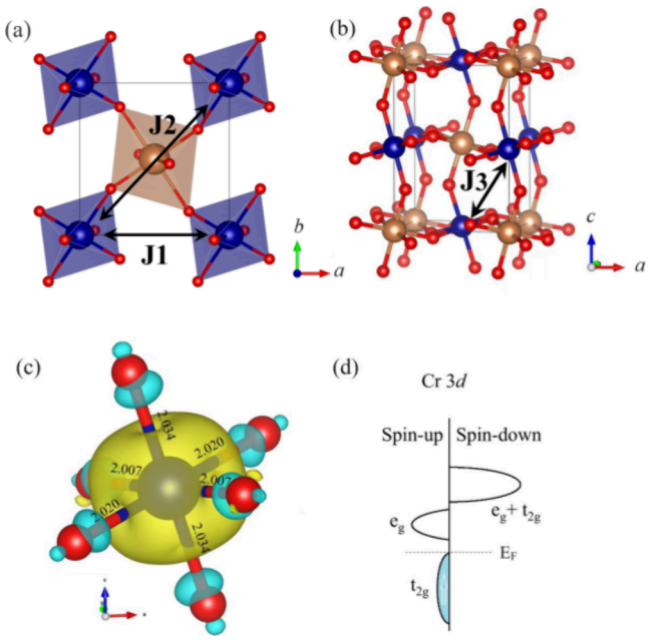

Figure 8. (a, b) Schematic diagram of the Cr exchange paths. (c) 3D magnetic charge density corresponding to the Cr. Blue, brown, and red atoms represent Cr, Cd, and O, respectively. Yellow (cyan) isosurface corresponds to the predominant spin-up (spin-down) charge density of +0.004 e/Å^3 (−0.004 e/Å^3). (d) Schematic configuration of the Cr 3*d* orbital in CCSO.

considerable mixture between the t_{2g} and e_g orbitals, leaving some empty states on the t_{2g} orbital. As a consequence, the virtual hopping $t_{2g}\uparrow$-$t_{2g}\uparrow$ is allowed and dominated, and therefore, the FM state forms for Ca_2CrSbO_6. In the current CCSO, the Cr−O−Sb angle is further decreased to 147.5° (Figure 8a), and the larger tilting of octahedra decreases the Cr−O−Sb bond angle and increases the superexchange between the half-filled t_{2g} electrons of the Cr atom, especially in the *z* direction (J_3). It is this enhanced virtual hopping $t_{2g}\uparrow$ -$t_{2g}\uparrow$ interaction that increases the magnetic interaction between Cr atoms and further stabilize the FM state in CCSO. As a result, the T_C is enhanced from 13 K in Ca_2CrSbO_6 to 16.5 K in CCSO.

CCSO provides a desirable example of intrinsic FM insulator with a considerable band gap of about 1.55 eV, which in principle transports only the spin momentum without charge carrier. The FM order and the insulating state are usually mutual exclusive because the FM is relevant to the actual hopping of the electrons, e.g., double exchange[43,44] or RKKY mechanism,[45,46] resulting in the delocalization of the electrons as well as metallic property. In CCSO, however, the long-range superexchange interactions between Cr^{3+} with virtual electron hoping ensure the concurrence of FM and insulating features with an enhanced Curie temperature compared to that of the isostructural Ca_2CrSbO_6. The intrinsic ferromagnetic and insulating nature makes CCSO a promising candidate for low-temperature spintronics applications.[27−30]

4. CONCLUSIONS

In summary, a novel B-site ordered double perovskite oxide Cd_2CrSbO_6 was synthesized at 9 GPa and 1375 K. It crystallizes to $P2_1/n$ space group with smaller Cd residing at the A-site and Cr and Sb occupying the B-site in a rock salt fashion. The charge configuration is confirmed to be Cd^{2+}/Cr^{3+}/Sb^{5+}. Although the magnetic Cr^{3+} ions form a tetrahedral structural frustrated lattice, Cd_2CrSbO_6 experiences a long-range ferromagnetic phase transition at 16.5 K. The heavier Cr/SbO_6 tilting leads to the mixture of the Cr t_{2g} and e_g orbitals and thus enables the ferromagnetic superexchange through the Cr−O−Cd−O−Cr pathway, leading to the presence of an enhanced Curie temperature compared to that of Ca_2CrSbO_6. In addition, Cd_2CrSbO_6 shows electrical insulating behavior, with a considerable band gap of 1.55 eV.

■ ASSOCIATED CONTENT

Accession Codes

CCDC 2378671 contains the supplementary crystallographic data for this paper. These data can be obtained free of charge via www.ccdc.cam.ac.uk/data_request/cif, or by emailing data_request@ccdc.cam.ac.uk, or by contacting The Cambridge Crystallographic Data Centre, 12 Union Road, Cambridge CB2 1EZ, UK; fax: +44 1223 336033.

■ AUTHOR INFORMATION

Corresponding Authors

Jiawang Hong − *School of Aerospace Engineering, Beijing Institute of Technology, Beijing 100081, China;* orcid.org/0000-0002-9915-8072; Email: hongjw@bit.edu.cn

Zhenhua Chi − *Institute of Plasma Physics, HFIPS, Chinese Academy of Sciences, Hefei 230031, China*; Email: zhchi@issp.ac.cn

Youwen Long − *Beijing National Laboratory for Condensed Matter Physics, Institute of Physics, Chinese Academy of Sciences, Beijing 100190, China; School of Physical Sciences, University of Chinese Academy of Sciences, Beijing 100049, China; Songshan Lake Materials Laboratory, Dongguan, Guangdong 523808, China;* orcid.org/0000-0002-8587-7818; Email: ywlong@iphy.ac.cn

Authors

Shengjie Liu − *Beijing National Laboratory for Condensed Matter Physics, Institute of Physics, Chinese Academy of Sciences, Beijing 100190, China; Institute of High Pressure Physics, School of Physical Science and Technology, Ningbo University, Ningbo 315211, China*

Xiao Wang − *Beijing National Laboratory for Condensed Matter Physics, Institute of Physics, Chinese Academy of Sciences, Beijing 100190, China;* orcid.org/0000-0001-8139-4192

Zunyi Deng − *School of Aerospace Engineering, Beijing Institute of Technology, Beijing 100081, China*

Xubin Ye − *Beijing National Laboratory for Condensed Matter Physics, Institute of Physics, Chinese Academy of Sciences, Beijing 100190, China;* orcid.org/0000-0002-5739-8318

Zhao Pan − *Beijing National Laboratory for Condensed Matter Physics, Institute of Physics, Chinese Academy of Sciences, Beijing 100190, China;* orcid.org/0000-0002-8693-2508

Dabiao Lu − *Beijing National Laboratory for Condensed Matter Physics, Institute of Physics, Chinese Academy of Sciences, Beijing 100190, China; School of Physical Sciences, University of Chinese Academy of Sciences, Beijing 100049, China;* orcid.org/0009-0006-5489-2835

Haoting Zhao − *Beijing National Laboratory for Condensed Matter Physics, Institute of Physics, Chinese Academy of Sciences, Beijing 100190, China; School of Physical Sciences,*

https://doi.org/10.1021/acs.inorgchem.4c03543
Inorg. Chem. 2024, 63, 19964−19971

University of Chinese Academy of Sciences, Beijing 100049, China; orcid.org/0009-0007-9656-5709

Jie Zhang − *Beijing National Laboratory for Condensed Matter Physics, Institute of Physics, Chinese Academy of Sciences, Beijing 100190, China; School of Physical Sciences, University of Chinese Academy of Sciences, Beijing 100049, China;* orcid.org/0009-0006-9055-2969

Maocai Pi − *Beijing National Laboratory for Condensed Matter Physics, Institute of Physics, Chinese Academy of Sciences, Beijing 100190, China; School of Physical Sciences, University of Chinese Academy of Sciences, Beijing 100049, China*

Zhiwei Hu − *Max Planck Institute for Chemical Physics of Solids, 01187 Dresden, Germany;* orcid.org/0000-0003-0324-2227

Chien-Te Chen − *National Synchrotron Radiation Research Center (NSRRC), Hsinchu 300092, Taiwan*

Cheng Dong − *Beijing National Laboratory for Condensed Matter Physics, Institute of Physics, Chinese Academy of Sciences, Beijing 100190, China*

Yao Shen − *Beijing National Laboratory for Condensed Matter Physics, Institute of Physics, Chinese Academy of Sciences, Beijing 100190, China*

Tian Cui − *Institute of High Pressure Physics, School of Physical Science and Technology, Ningbo University, Ningbo 315211, China*

Yanping Huang − *Institute of High Pressure Physics, School of Physical Science and Technology, Ningbo University, Ningbo 315211, China*

Complete contact information is available at: https://pubs.acs.org/10.1021/acs.inorgchem.4c03543

Author Contributions

◆S. L. and X.W. contributed equally to this work.

Notes

The authors declare no competing financial interest.

■ ACKNOWLEDGMENTS

This work was supported by the National Key R&D Program of China (Grant No. 2021YFA1400300), the Beijing Natural Science Foundation (Grant No. Z200007), the National Natural Science Foundation of China (Grants No. 11934017, 12261131499, 11921004, 12304159, 12304268), the China Postdoctoral Science Foundation (Grant No. 2023M743741), the Chinese Academy of Sciences (Grant No. XDB33000000), and Beijing National Laboratory for Condensed Matter Physics (2023BNLCMPKF003). The synchrotron x-ray diffraction experiments were performed at SPring-8 with the approval of the Japan Synchrotron Radiation Research Institute (2023B1575, 2023B1976, 2024A1506, 2024A1695).

■ REFERENCES

(1) Vasala, S.; Karppinen, M. $A_2B'B''O_6$ perovskites: a review. *Prog. Solid State Chem.* **2015**, *43* (1), 1.

(2) Kobayashi, K. I.; Kimura, T.; Sawada, H.; Terakura, K.; Tokura, Y. Room-temperature magnetoresistance in an oxide material with an ordered double-perovskite structure. *Nature* **1998**, *395* (6703), 677.

(3) Zhao, H.; Pan, Z.; Shen, X.; Zhao, J.; Lu, D.; Zhang, J.; Hu, Z.; Kuo, C. Y.; Chen, C. T.; Chan, T. S. Antiferroelectricity-induced negative thermal expansion in double perovskite Pb_2CoMoO_6. *Small* **2024**, *20* (2), No. 2305219.

(4) Deng, Z.; Wang, X.; Wang, M. Q.; Shen, F.; Zhang, J.; Chen, Y. S.; Feng, H. L.; Xu, J. W.; Peng, Y.; Li, W. M. Giant exchange-bias-like effect at low cooling fields induced by pinned magnetic domains in Y_2NiIrO_6 double perovskite. *Adv. Mater.* **2023**, *35* (17), No. 2209759.

(5) Chen, J.; Wang, X.; Hu, Z.; Tjeng, L. H.; Agrestini, S.; Valvidares, M.; Chen, K.; Nataf, L.; Baudelet, F.; Nagao, M.; et al. Enhanced magnetization of the highest-T_C ferrimagnetic oxide Sr_2CrOsO_6. *Phys. Rev. B* **2020**, *102* (18), No. 184418.

(6) Wiebe, C. R.; Greedan, J. E.; Luke, G. M.; Gardner, J. S. Spin-glass behavior in the $S = 1/2$ fcc ordered perovskite Sr_2CaReO_6. *Phys. Rev. B* **2002**, *65* (14), No. 144413.

(7) Wiebe, R.; Greedan, E.; Kyriakou, P.; Luke, M.; Gardner, S.; Fukaya, A.; Gat-Malureanu, M.; Russo, L.; Savici, T.; Uemura, J. Frustration-driven spin freezing in the $S = 1/2$ fcc perovskite Sr_2MgReO_6. *Phys. Rev. B* **2003**, *68* (13), No. 134410.

(8) Stitzer, K. E.; Smith, M. D.; Zur Loye, H. C. Crystal growth of Ba_2MOsO_6 (M = Li, Na) from reactive hydroxide fluxes. *Solid State Sci.* **2002**, *4* (3), 311−316.

(9) Aharen, T.; Greedan, J. E.; Bridges, C. A.; Aczel, A. A.; Rodriguez, J.; MacDougall, G.; Luke, G. M.; Imai, T.; Michaelis, V. K.; Kroeker, S.; Zhou, H.; Wiebe, C. R.; Cranswick, L. M. D. Magnetic properties of the geometrically frustrated $S = 1/2$ antiferromagnets, La_2LiMoO_6 and Ba_2YMoO_6, with the B-site ordered double perovskite structure: evidence for a collective spin-singlet ground state. *Phys. Rev. B* **2010**, *81* (22), No. 224409.

(10) King, G.; Thimmaiah, S.; Dwivedi, A.; Woodward, P. M. Synthesis and characterization of new $AA'BWO_6$ perovskites exhibiting simultaneous ordering of A-site and B-site cations. *Chem. Mater.* **2007**, *19* (26), 6451−6458.

(11) Aharen, T.; Greedan, J. E.; Ning, F.; Imai, T.; Michaelis, V.; Kroeker, S.; Zhou, H.; Wiebe, C. R.; Cranswick, L. M. D. Magnetic properties of the $S = 3/2$ geometrically frustrated double perovskites La_2LiRuO_6 and Ba_2YRuO_6. *Phys. Rev. B* **2009**, *80* (13), No. 134423.

(12) Aharen, T.; Greedan, J. E.; Bridges, C. A.; Aczel, A. A.; Rodriguez, J.; MacDougall, G.; Luke, G. M.; Michaelis, V. K.; Kroeker, S.; Wiebe, C. R.; Zhou, H.; Cranswick, L. M. D. Structure and magnetic properties of the $S = 1$ geometrically frustrated double perovskites La_2LiReO_6 and Ba_2YReO_6. *Phys. Rev. B* **2010**, *81* (6), No. 064436.

(13) Young, J.; Stroppa, A.; Picozzi, S.; Rondinelli, J. M. Tuning the ferroelectric polarization in $AA'MnWO_6$ double perovskites through A cation substitution. *Dalt. Trans.* **2015**, *44* (23), 10644−10653.

(14) Moessner, R.; Ramirez, A. P. Geometrical frustration. *Phys. Today* **2006**, *59* (2), 24.

(15) Karunadasa, H.; Huang, Q.; Ueland, B.; Schiffer, P.; Cava, R. Ba_2LnSbO_6 and Sr_2LnSbO_6 (Ln = Dy, Ho, Gd) double perovskites: lanthanides in the geometrically frustrating fcc lattice. *Proc. Natl. Acad. Sci. U. S. A.* **2003**, *100* (14), 8097.

(16) Calder, S.; Ke, X.; Bert, F.; Amato, A.; Baines, C.; Carboni, C.; Cava, R. J.; Daoud-Aladine, A.; Deen, P.; Fennell, T.; et al. Magnetic properties of Ba_2HoSbO_6 with a frustrated lattice geometry. *Phys. Rev. B* **2010**, *81* (6), No. 064425.

(17) Mustonen, O.; Vasala, S.; Sadrollahi, E.; Schmidt, K.; Baines, C.; Walker, H.; Terasaki, I.; Litterst, F.; Baggio-Saitovitch, E.; Karppinen, M. Spin-liquid-like state in a spin-1/2 square-lattice antiferromagnet perovskite induced by d^{10}−d^0 cation mixing. *Nat. Commun.* **2018**, *9* (1), 1085.

(18) Ivanov, S.; Nordblad, P.; Tellgren, R.; Hewat, A. Temperature evolution of structure and magnetic properties in the perovskite Sr_2MnSbO_6. *Mater. Res. Bull.* **2009**, *44* (4), 822.

(19) Cussen, E. J.; Vente, J. F.; Battle, P. D.; Gibb, T. C. Neutron diffraction study of the influence of structural disorder on the magnetic properties of Sr_2FeMO_6 (M = Ta, Sb). *J. Mater. Chem.* **1997**, *7* (3), 459.

(20) Retuerto, M.; Garcia-Hernandez, M.; Martínez-Lope, M.; Fernandez-Diaz, M.; Attfield, J.; Alonso, J. Switching from ferro-to antiferromagnetism in A_2CrSbO_6 (A = Ca, Sr) double perovskites: a neutron diffraction study. *J. Mater. Chem.* **2007**, *17* (33), 3555.

(21) Retuerto, M.; Alonso, J.; García-Hernández, M.; Martínez-Lope, M. Synthesis, structure and magnetic properties of the new double perovskite Ca_2CrSbO_6. *Solid State Commun.* **2006**, *139* (1), 19.
(22) Baidya, S.; Saha-Dasgupta, T. Effect of A cation on magnetic properties of double perovskite compounds: from ferromagnetic Ca_2CrSbO_6 to antiferromagnetic Sr_2CrSbO_6. *Phys. Rev. B* **2012**, *86*, No. 024440.
(23) Ishida, K.; Tassel, C.; Watabe, D.; Takatsu, H.; Brown, C. M.; Nilsen, G. J.; Kageyama, H. Spin frustration in double perovskite oxides and oxynitrides: enhanced frustration in La_2MnTaO_5N with a large octahedral rotation. *Inorg. Chem.* **2021**, *60* (11), 8252.
(24) Li, M. R.; Retuerto, M.; Deng, Z.; Stephens, P. W.; Croft, M.; Huang, Q. Z.; Wu, H.; Deng, X. Y.; Kotliar, G.; Sánchez-Benítez, J. Giant magnetoresistance in the half-metallic double-perovskite ferrimagnet Mn_2FeReO_6. *Angew. Chem., Int. Ed.* **2015**, *54* (41), 12069.
(25) Long, Y.; Hayashi, N.; Saito, T.; Azuma, M.; Muranaka, S.; Shimakawa, Y. Temperature-induced A−B intersite charge transfer in an A-site-ordered $LaCu_3Fe_4O_{12}$ perovskite. *Nature* **2009**, *458* (7234), 60.
(26) Zhang, J.; Liu, Z. H.; Ye, X. B.; Wang, X.; Lu, D. D.; Zhao, H. T.; Pi, M. C.; Chen, C.-T.; Chen, J.-L.; Kuo, C.-Y. High-pressure synthesis of quadruple perovskite oxide $CaCu_3Cr_2Re_2O_{12}$ with a high ferrimagnetic Curie temperature. *Inorg. Chem.* **2024**, *63* (7), 3499.
(27) Katmis, F.; Lauter, V.; Nogueira, F. S.; Assaf, B. A.; Jamer, M. E.; Wei, P.; Satpati, B.; Freeland, J. W.; Eremin, I.; Heiman, D. A high-temperature ferromagnetic topological insulating phase by proximity coupling. *Nature* **2016**, *533* (7604), 513.
(28) Zhao, H.; Bai, Y.; Yin, K.; Wang, X.; Liu, Z.; Ye, X.; Lu, D.; Zhang, J.; Pi, M.; Hu, Z. $CaCu_3Mn_2Te_2O_{12}$: an intrinsic ferrimagnetic insulator prepared under high pressure. *Inorg. Chem.* **2023**, *62* (51), 21233.
(29) Jiang, S.; Li, L.; Wang, Z.; Shan, J.; Mak, K. F. Spin tunnel field-effect transistors based on two-dimensional van der Waals heterostructures. *Nat. Electron.* **2019**, *2* (4), 159.
(30) Ferreira, G. J.; Loss, D. Magnetically defined qubits on 3D topological insulators. *Phys. Rev. Lett.* **2013**, *111* (10), No. 106802.
(31) Von Dreele, R. Quantitative texture analysis by Rietveld refinement. *J. Appl. Crystallogr.* **1997**, *30* (4), 517.
(32) Kresse, G.; Hafner, J. Ab initio molecular dynamics for liquid metals. *Phys. Rev. B* **1993**, *47* (1), 558.
(33) Kresse, G.; Furthmüller, J. Efficiency of ab-initio total energy calculations for metals and semiconductors using a plane-wave basis set. *Comput. Mater. Sci.* **1996**, *6* (1), 15.
(34) Kresse, G.; Furthmüller, J. Efficient iterative schemes for ab initio total-energy calculations using a plane-wave basis set. *Phys. Rev. B* **1996**, *54* (16), 11169.
(35) Kresse, G.; Joubert, D. From ultrasoft pseudopotentials to the projector augmented-wave method. *Phys. Rev. B* **1999**, *59* (3), 1758.
(36) Perdew, J. P.; Burke, K.; Ernzerhof, M. Generalized gradient approximation made simple. *Phys. Rev. Lett.* **1996**, *77* (18), 3865.
(37) Momma, K.; Izumi, F. VESTA: a three-dimensional visualization system for electronic and structural analysis. *J. Appl. Crystallogr.* **2008**, *41* (3), 653.
(38) Brown, I. D.; Altermatt, D. Bond-valence parameters obtained from a systematic analysis of the inorganic crystal structure database. *Acta. Cryst. B* **1985**, *41* (4), 244.
(39) Zhao, J.; Haw, S.-C.; Wang, X.; Cao, L.; Lin, H.-J.; Chen, C.-T.; Sahle, C. J.; Tanaka, A.; Chen, J.-M.; Jin, C.; et al. Stability of the Pb divalent state in insulating and metallic $PbCrO_3$. *Phys. Rev. B* **2023**, *107* (2), No. 024107.
(40) Kittel, C. *Introduction to solid state physics*, 8th ed.; John Wiley & Sons, 2005; Chapter 5, pp. 105−130.
(41) Li, B.; Ye, X.; Wang, X.; Zhang, J.; Lu, D.; Zhao, H.; Pi, M.; Hu, Z.; Lin, H.-J.; Chen, C.-T. High-pressure-stabilized post-spinel phase of $CdFe_2O_4$ with distinct magnetism from its ambient-pressure spinel phase. *Inorg. Chem.* **2023**, *62* (23), 9139.
(42) Shklovskii, B. I.; Efros, A. L. *Electronic properties of doped semiconductors*; Springer-Verlag: Berlin Heidelberg GmbH, 1984; Chapter 9, pp. 202−227.
(43) Anderson, P. W.; Hasegawa, H. Considerations on double exchange. *Phys. Rev.* **1955**, *100* (2), 675.
(44) Millis, A.; Shraiman, B. I.; Mueller, R. Dynamic Jahn-Teller effect and colossal magnetoresistance in $La_{1-x}Sr_xMnO_3$. *Phys. Rev. Lett.* **1996**, *77* (1), 175.
(45) Zhao, Y. J.; Shishidou, T.; Freeman, A. Ruderman-Kittel-Kasuya-Yosida−like ferromagnetism in Mn_xGe_{1-x}. *Phys. Rev. Lett.* **2003**, *90* (4), No. 047204.
(46) Matsukura, F.; Ohno, H.; Shen, A.; Sugawara, Y. Transport properties and origin of ferromagnetism in (Ga,Mn)As. *Phys. Rev. B* **1998**, *57* (4), R2037.

https://doi.org/10.1021/acs.inorgchem.4c03543
Inorg. Chem. 2024, 63, 19964−19971